B2. Dual-Polarized Chipless RFID Tag with Temperature Sensing Capability

S.H. Zainud-Deen[1], M. A. Abo-Elhassan[1], H.A. Malhat[1], and K.H. Awadalla[1].*
[1]Faculty of Electronic Eng., Menoufia University, Egypt. *er_honida1@yahoo.com

ABSTRACT

In this paper dual-polarized chipless RFID tag with temperature sensing capability is proposed. The tag is constructed by incorporating a V-polarized and H-polarized slots containing either same or different code to increase the tag data capacity. The tag is having dual performance of tagging and temperature sensing simultaneously. The integration of temperature sensing is performed by utilizing the resonant frequency of a specific slot of the tag to represent the sensor change parameter. Different encoding techniques for different codes arrangement has been presented. The radiation characteristics of the chipless tag are investigated and analyzed using the finite element method and are compared with that obtained by the finite integration technique.

Keywords: *Slot antenna, Chipless RFID, Dual polarization, Temperature sensing.*

I. INTRODUCTION

Radio frequency identification (RFID) provides wireless identification and tracking capability and is a technology more robust than barcode [1]. RFID systems provide an automatic means to identify physical objects without the need for line-of-sight communication. The main components of RFID system are tag, reader, and host computer. RFID tag is attached to physical object as a means to identify the object. RFID readers convert the radio waves sent back from the tags to get the digital data and send the collected data to the host computer. In spite of the numerous advantages of conventional RFID system like long read range and high storage capacity of data, its growth has been slow mainly because of economic reasons [2]. These limitations have been solved by the development of chipless RFID tags [3]. Recently, chipless RFID tags have become very interesting in research area for low cost commercial applications. It does not contain any silicon chip, thus reducing the design complexity of the tag. The principle of information encoding is based on the generation of a specific frequency signature for each product i.e. wireless barcode. The chipless tag usually contains some planar circuits which will reflect the reader's signal back. This unique reflected signal can be used as the object identifier, a concept very similar to the principle of radar [4]. The data is electromagnetically coded in the amplitude or phase of the wave. Different kinds of tags that are based on amplitude-frequency signature have been developed in [5]. In chipless RFID tags, resonators are used to encode the data and polarization diversity is used to isolate interrogation signal and the backscattered signal. Since this is based on the amplitude variations, there are possibilities of error in a noisy environment and in this context, phase based coding has more significance. For implementing this structure as a chipless tag, receiving and transmitting antennas have been added. The entire system has been simulated. The backscattered signal from the tag has been used for the encoding purpose. A number of printable chipless RFID tags have been reported in the literature. The reported analysis was using time-domain, frequency-domain, phase-domain, and image-based encoding techniques. A chipless tag using spiral resonators has been used in [6], but the size of the tag increases with the increase in the number of bits. For the frequency-domain-based tags, it is observed that they have higher data density than time-domain-based tags, and a 35-bit tag using spiral resonators and cross-polarized monopole antennas in the frequency domain has already been presented in [6]. A multiresonant dipole antenna (MRDA) was attached to a monopole antenna to encode bits in [7]. However, it requires dual-side printing alignment and the number of dipoles increases linearly with the number of bits. A chipless tag using capacitively tuned dipoles in [8] has problems with size and parasitic mutual coupling. Another printable tag using a space-filling curve [9] has difficulties in encoding data.

Some smart functionality have been added to the classical RFID systems such as, sensing which can be implemented into a chipless RFID [10, 11]. In the literature, some chipless sensors are able to detect ethylene gas [10]. In chipless RFID tag, the sensor is used by implementing the change in the sensor parameter either to the tag antenna or to the ID code generation circuit.

This paper presents a proposed radio frequency identification chipless tag that is highly compact and potentially low cost. This tag has a lot of advantages, such as being fully printable on products since no ground plane is required for fabrication, and only conductive layer is needed. Resonant frequencies can be shifted by setting an additional short circuit at particular locations. A compact easily-printable arc shaped slot-loaded dual

978-1-4799-3821-6/14/$31.00 ©2014 IEEE

polarized chipless tag is introduced. This tag can be used as an orientation independent tag at the half data capacity of the dual polarized tag. It will overcome the bandwidth limitation with dual polarized setup by encoding double number of bits in UWB frequency band. A tag dimensions of 40×40 mm^2 with 30 bits capacity is encoded in the frequency band from 4 to16 GHz. A novel chipless RFID temperature sensor is integrated with the tag to end up having dual performance of tagging and temperature sensing simultaneously. Results verify that the sensing mechanism is independent of identifying the object. The chipless tag is designed and analyzed using the finite element method (FEM) [12] and are compared with results obtained by the finite integration technique (FIT) [13].

II. THEORY OF OPERATION

The tag slots are selected relatively thin to have a narrow bandwidth. This is optimized to reduce the coupling effect of such close slots. Therefore, as the bandwidth of each slot is kept narrow and not overlapping with the neighbouring slots, the coupling effect is minimized. Each slot corresponds to one bit in the frequency domain response of the tag. There are two groups of slots, one group is for the vertical polarization response and the other group is for the horizontal polarization response. The resonant frequency (f) of a half-wave slot-line resonator with a physical length of l can be approximated as [14]

$$f = \frac{c}{2l}\sqrt{\frac{2}{\varepsilon_r+1}} \quad (1)$$

where c is the speed of light in free space and ε_r is the relative permittivity of the substrate.

Since, the H-polarized slots will not respond to the V-polarized plane wave and vice versa; both V-and H-polarized slots can be placed in a single tag and interrogated with dual-polarized waves as shown in Fig.1. When the tag is excited by a dual-polarized transmit antenna (Tx), the frequency-encoded backscattered signal from the tag is received by another dual-polarized receive antenna (Rx) as shown in Fig. 1. The V–polarized receiver (V_r) will receive the frequency encoded signal from the V- polarized slots of the tag, since they show frequency response only to the V-polarized transmitted signal (V_r). Similarly the H–polarized receiver (H_r) will receive the frequency encoded signal from the H-polarized slots, which respond only to the H-polarized transmitted signal (H_t).

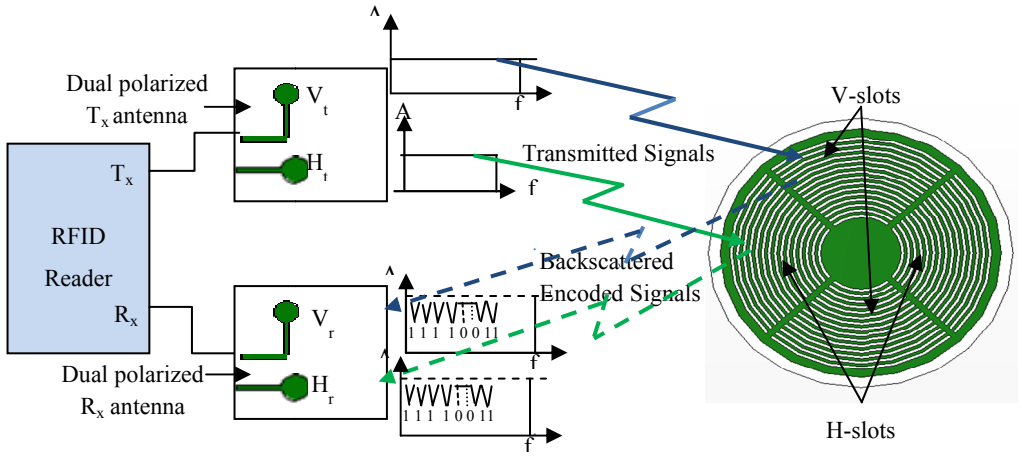

Fig.1: Principle of operation of the proposed chipless RFID tag.

III. NUMERICAL RESULTS

A. Single polarized tag

A single-sided compact chipless tag with arc-shaped slot is shown in Fig.2a. The tag consists of a circular substrate disk with ε_r=2.5, radius R_s=19.5 mm and thickness h=0.5 mm. A printed circular metallic patch with radius R_p=18 mm, one arc-shaped slot with width W_s=0.4 mm and arc radius R_1 =16.8 mm and subtending an angle from 46°< Φ_0 < 134° is placed at the top of the tag substrate disk and there is no ground plane on the

opposite face of the substrate disk. The backscattered field (i.e. RCS) for H-polarized plane wave that is used for the excitation of the tag (H-polarized slot) is shown in Fig.2b. The RCS results shows a deep notch resonance at 4.75 GHz with 3-dB BW of 250 MHz and there are no other resonance throughout the band up to 20 GHz. Theoretical resonance frequency calculated using eq .1 is 4.39 GHz which is approximately the same as that obtained by simulation. Similarly, the backscattered RCS response from the tag when excited by a V-polarized plane wave is shown in Fig.2c. The tag has no response (no notch resonance) to the V-polarized plane wave as it appeared from the RCS component. The RCS response is calculated using the FIT technique and confirmed using the FEM method which shows good agreement between results.

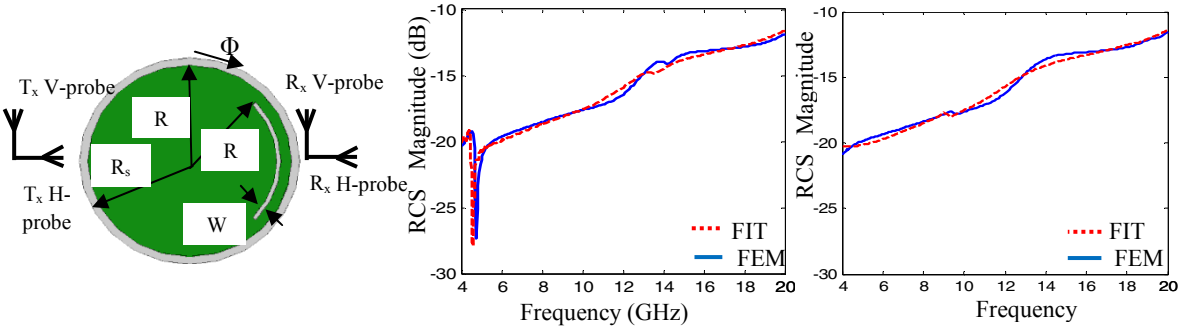

a. Geometry b. H-polarized plane wave c. V-polarized plane wave

Fig.2 (a) Circular patch loaded with an arc-shaped slot.
(b) Backscattered frequency response for H- Polarized plane wave.
(c) Backscattered frequency response for V-Polarized plane wave.

B. Dual polarized tag

Two similar sets of slots are etched in the copper disk such that one is horizontally and the other is vertically polarized to double the number of bits within the same frequency bandwidth. In addition, to increase the effect of each set of slots by increasing the reflection, each group of slots is mirror copied on the opposite side of the tag as shown in Fig. 1. This construction will overcome the bandwidth limitations that exist in a single polarity tags and doubles the data encoding capacity for the frequency-domain-based tags. The geometry of a 30-bit arc-shaped slotted patch is shown in Fig.3a. The design parameters are: R_p = 18 mm is the radius of the patch, R_1 =16.8 mm is the radius of the longest arc-resonator, R_{15} = *5.2 mm* is the radius of the shortest arc-resonator, S_s =*0.4 mm* is the separation between two successive slots, W_s =*0.4 mm* is the width of each slot, and G = 0.8 mm is the gap between H and V- polarized slots. The arc-shaped slot lengths are different, so that different frequency signatures are obtained. W_s and S_s are kept the same for every arc-shaped slot resonator irrespective of its length. The tag is placed on Taconic TLX-9 substrate with permittivity, ε_r = 2.5, thickness, h =0.5 mm and loss tangent, tan δ = 0.0019. The tag is designed to operate in frequency band from 4 to 16 GHz. The RCS variation versus frequency of the structure when illuminated by H/V polarized plane wave is shown in Fig.3b. The 30-bit tag has all bits are set to 1's. Two identical sets of 15 V-slots of different lengths show response in the V-probe receiver and another two identical sets of 15 H-slots (At the left and the right) of different length show response in the H-probe receiver, where we can see 15 dips in both the V-and H-probe receivers response as shown in Fig. 3b.

The frequency signatures can be modified by just removing (or shorting) the slots which will move the resonant frequencies of the slots out of the frequency band of interest as shown in the different configurations appeared in Fig.4 and Fig.5. Eight slots are removed (shorted) from the 15 V-slots in the tag of Fig.4a, Fig.5a and their corresponding frequency response in the V-probe receiver in Fig.4b, Fig.5b have disappeared, which are denoted as logic '0's. Similarly, seven H-slots are removed (shorted) from the 15 H-slots of the tag and seven notches have disappeared from the H-probe response as shown in Fig.4b. Due to the mutual coupling between the slots, there is a very little shift in the adjacent frequencies after the shorting of the slots.

C. Effect of the Tag Rotation on tag Performance

The tag of 7 operating V-slots and 8 operating H-slots are used in this section. The effect of tag rotation (Fig.6) on the RCS frequency response is to be investigated. If the tag (slots) is rotated by an angle φ, the incident V-polarized plane wave will be picked up partially by the H-slots. This is due to the fact that the incident vertically polarized electric field will have a component parallel to the main polarization axes of the H-slots in its new

orientation. As a result, H-slots will respond to the V-polarized wave and the V-probe receiver will receive the combined response from both H-and V-slots and vice versa. Figure 7 shows RCS variation versus frequency for rotated tags response to the V/H-polarized waves at different rotation angles. If the rotation angle is small, the cross-polar response due to the effect of the cross-polar slots will also be small. However, if the rotation angle increases the cross-polar response increases too. At 45° rotation angle, the response from the cross-polar component becomes equal to the response from the co-polar component. Hence, dual-polarization tag can be used up to a certain degree. From the obtained results, it is recommended to be not more than ±30° of tag rotation. The simulation results for the tags of Fig.6b with 40 degrees rotation are predicted in Fig.7c.The Figure indicates that both the V-slots response and the H-slots response are so weak to become unreadable.

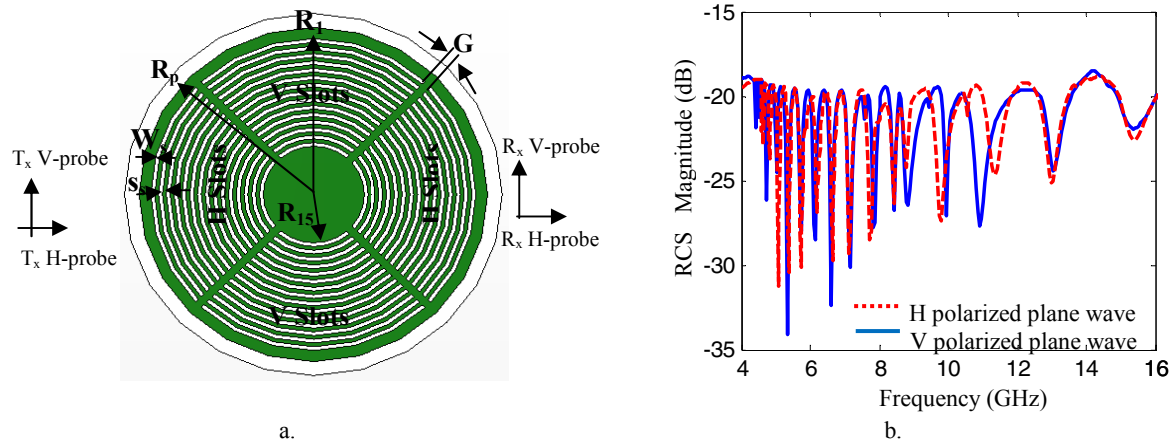

a. b.

Fig.3 (a) The geometry of 30-bit slotted loaded circular patch tag.
(b)The simulated RCS variation versus frequency for the 30-bit slotted loaded circular patch tag.

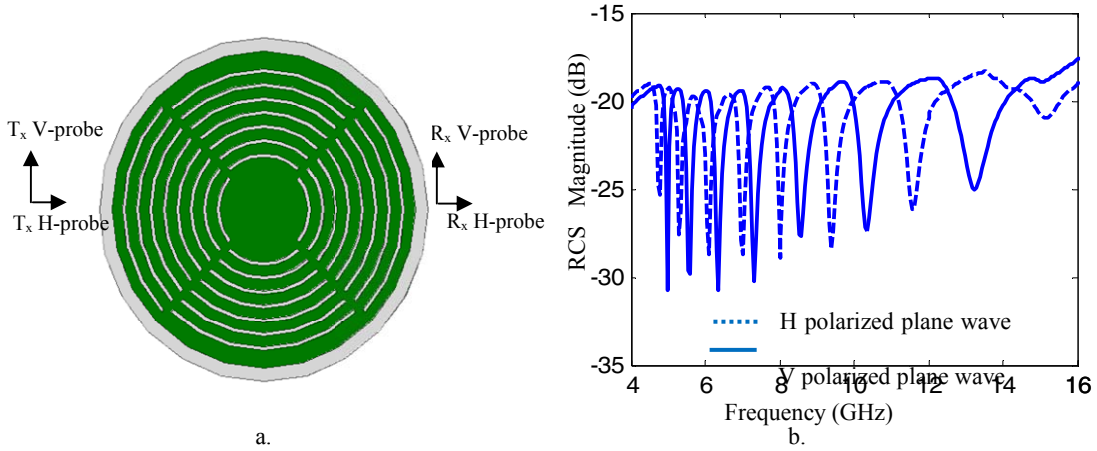

a. b.

Fig.4: (a) The geometry of 30 bit dual polarized tag with eight 0's in V polarization and seven 0's in H polarization.
(b) The simulated RCS variation versus frequency for the tag with different code.

D. Tag as a temperature sensor

In chipless RFID tag, the temperature sensor is generally used by implementing the change in the sensor parameter either to the tag antenna or to the ID code generation circuit. In this section, chipless RFID tag is proposed having dual performance of tagging and temperature sensing simultaneously. This tag structure, as described above, is actually integrating the tag antenna and the tag circuits. The used slots are fulfilling both functions. The simulated results verify that the temperature sensing mechanism in the proposed tag is independent of identifying the object. The integration of temperature sensing is performed by utilizing the resonant frequency of a specific slot of the tag to perform the sensor temperature affected parameter. Unlike earlier reported works on chipless RFID temperature sensors the proposed tag does not require any external circuitry or semiconductor chip for sensing environmental temperature. Rather, it performs real time temperature sensing using the dielectric property of temperature dependent high ε_r polyamides. Thus the first N-1 slots of N

bits tag can be used for data encoding whereas the N^{th} slot is the sensor for the temperature variation of the environment [15].

To incorporate temperature sensing, the arc-shaped slot having largest dimension was modified with Stanyl TE200F6 polyamide. Stanyl withstands high loads and stresses at high temperatures and exposure to aggressive environments [16]. Stanyl has the thermal expansion coefficient of (0.2×10^{-4}/°C) [17]. An outer slice of the Taconic TLX-9 substrate (α=12 ppm/°C [18]) is cut away and replaced with Stanyl as depicted in Fig. 8. This structural modification did not affect the adjacent slots thus their resonant condition remained unchanged. Stanyl polyamide has a linear variation of dielectric constant with temperature [15]. The top view of the modified slot is shown in Fig.8a. The slot having lowest resonant frequency is modified with Stanyl polyamide in the tag layout. Figure 8b shows the simulated resonance frequencies of the RCS response for different ε_r. It is observed that, with the variation of permittivity ε_r, the lowest resonance frequency shifts down accordingly while the other resonance frequencies remain constant. The variation of relative permittivity of Stanyl polyamide material versus temperature is shown in Fig.9a [19]. Hence, the shift of the resonance frequency of a single slot simulates the temperature variation and the other slots encode the data bits. Fig. 9b shows the simulated resonant frequencies for different ε_r. Correlating these two data, the temperature versus resonant frequency is extracted as shown in Fig.9c. The above relation can be fitted by the following equation, $T = p_1 f_r^3 + p_2 f_r^2 + p_3 f_r + p_4$ where $p_1 = -16155$, $p_2 = 2.0812 \times 10^5$, $p_3 = -8.9395 \times 10^5$ and $p_4 = 1.2803 \times 10^6$, where temperature T is in (degree centigrade) and the resonance frequency f_r is in (GHz). Hence, observing the resonant frequency of this particular slot the temperature information can be obtained. The material expansion for the arc slice made from Stanyl material is 3×10^{-5} meter and for a similar part made of the Taconic TLX-9 substrate material is 2×10^{-5} meter. The difference is 1×10^{-5} meter, which will not affect the complex substrate disk.

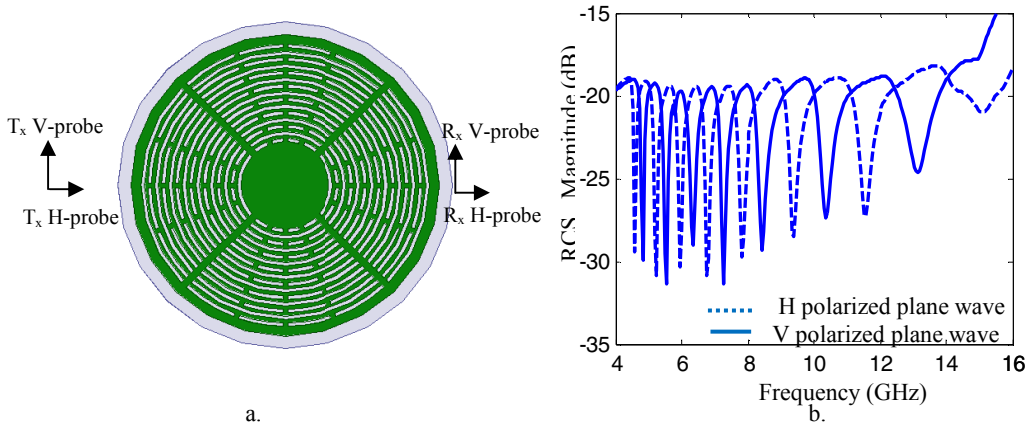

a. b.

Fig.5 (a) The geometry of 30 bit dual polarized tag with eight 0's in V polarization and seven 0's in H polarization.
(b) The simulated RCS variation versus frequency for the tag with different code.

IV. Conclusions

Chipless RFID tag has been designed. A dual polarized chipless tag is achieved by adding two sets of vertically polarized and horizontally polarized slots on the same tag to increase the tag data capacity. Different code configurations are designed by short circuiting slots in the tag to implement code bits as ones or zeros. A temperature sensing capability is added to the proposed tag by using temperature sensitive material placed on the most significant bit of the tag. A relationship between the resonance frequency of the sensor bit and the temperature variation have been worked out and presented.

References

[1] K. Finkelzeller, The RFID Handbook, Second Edition, John Wiley &Sons Ltd., London, UK, 2003.
[2] R. Want, "An introduction to RFID technology," IEEE Pervasive Computing, vol. 5, pp. 25-33, 2006.
[3] C. S. Hartmann, "A global SAW ID tag with large data capacity," Proceedings of 2002 IEEE Ultrasonics Symposium, Munich, Germany, pp. 65-69, Oct. 2002.
[4] Y. Huang and K. Boyle, Antennas from Theory to Practice, John Wiley & Sons, New York, USA, 2008.
[5] S. Preradovic and N. C. Karmakar, "Chipless RFID: barcode of the future," IEEE Microwave magazine vol. 11, pp. 87-97, Dec. 2010.

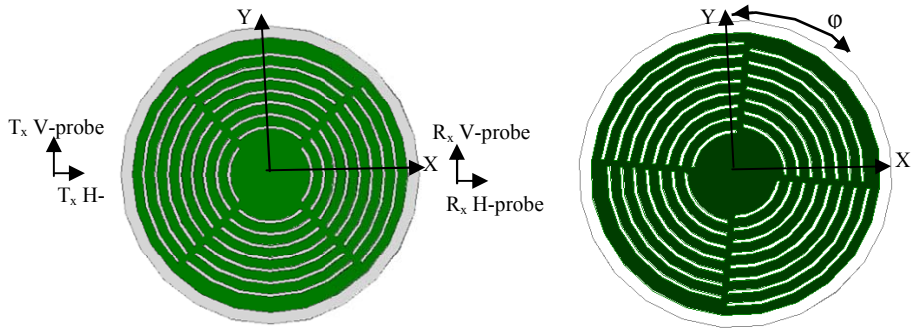

a. φ= 0◦ b. φ= 40◦

Fig. 6. Tag angle of rotation.

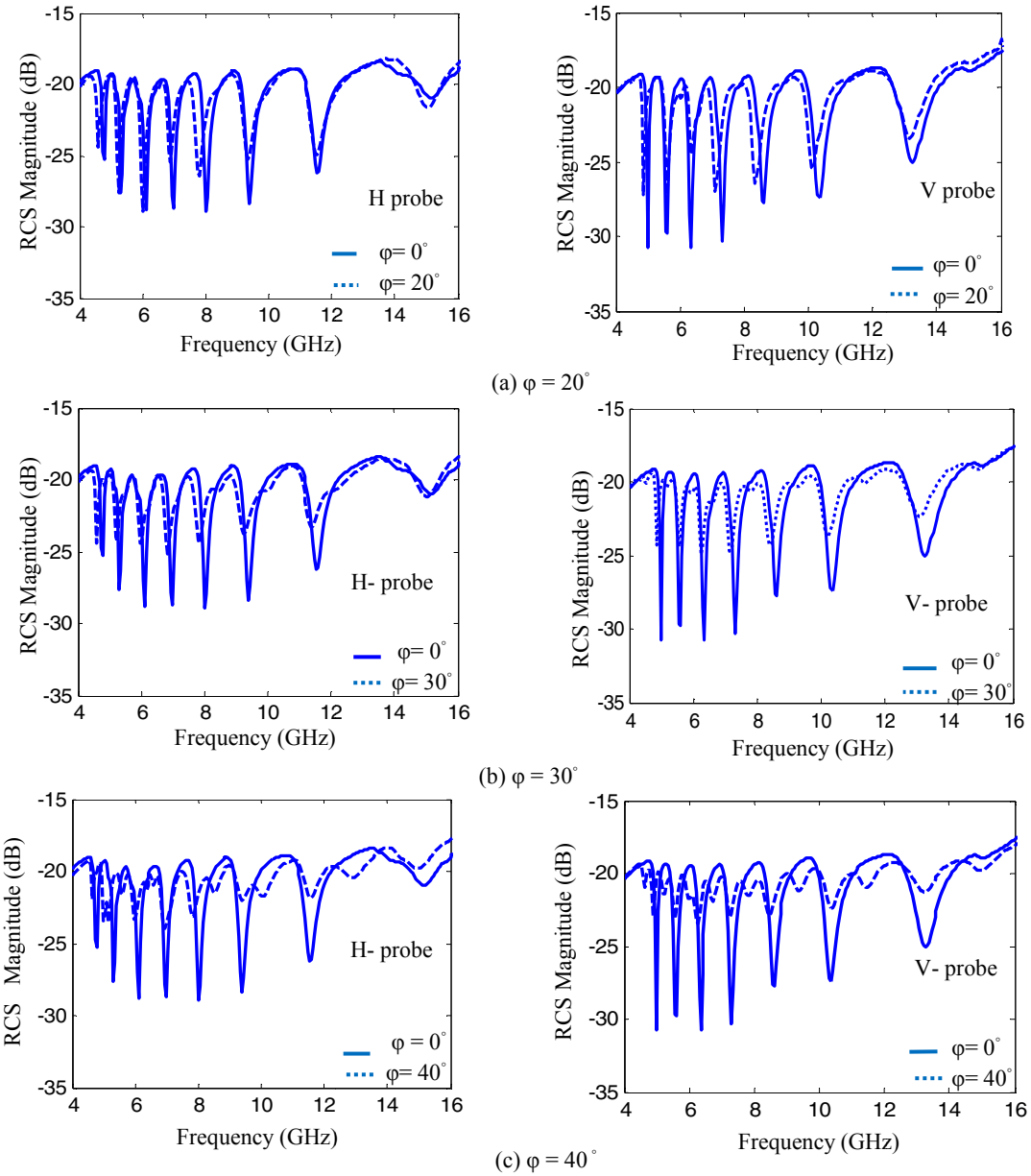

(a) φ = 20˚

(b) φ = 30˚

(c) φ = 40 ˚

Fig. 7: The RCS frequency response of the15 bit tag at different angles of rotation.

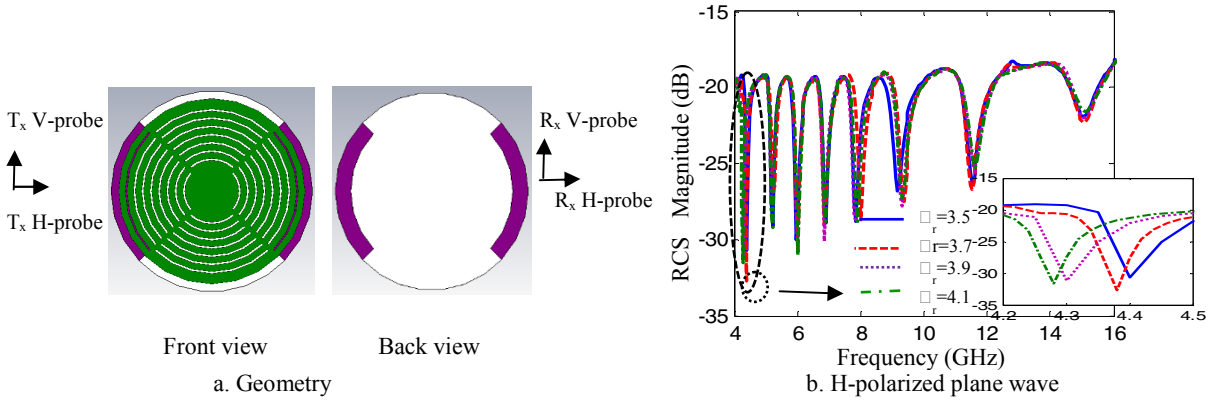

Fig. 8 (a) Geometry of modified first slot in the tag for temperature sensing capability.
(b) Simulated magnitude of RCS of the RFID tag with modified slot resonator versus frequency.

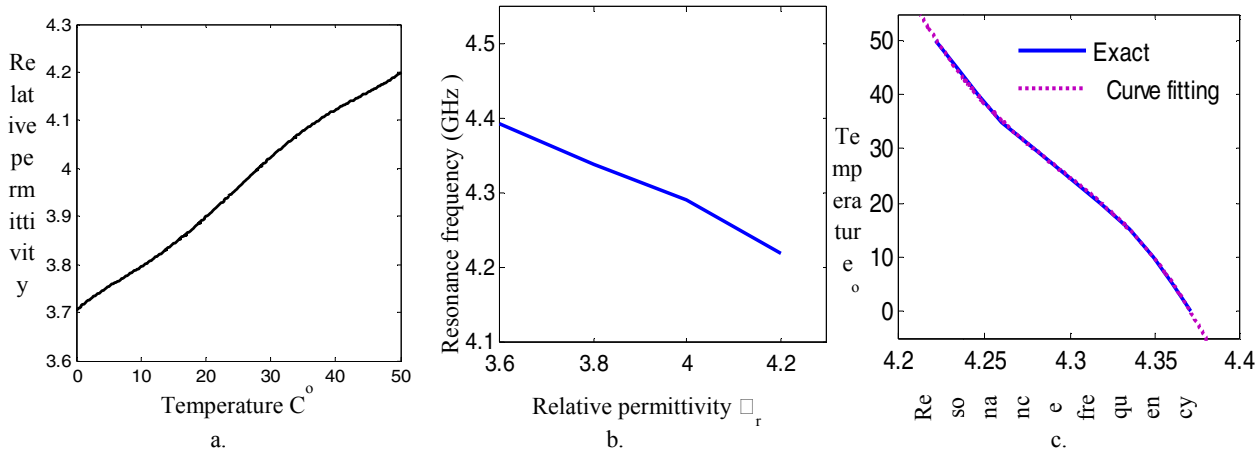

Fig. 9: (a) Measured ε_r versus temperature for Stanyl polyamide material [15].
(b) Simulated resonant frequency versus dielectric constant of Stanly material ε_r.
(c) Simulated temperature versus the first slot resonance frequency.

[6] S. Preradovic and N. C. Karmakar, "Design of fully printable planar chipless RFID transponder with 35-bit data capacity," Proc. European. Microwave Conference, pp. 013–016, Italy, Oct. 2009.
[7] I. Balbin and N. Karmakar, "Novel chipless RFID tag for conveyor belt tracking using multi-resonant dipole antenna," Proc. European. Microwave Conference, pp. 1109–1112, Italy, Oct, 2009.
[8] I. Jalaly and I. D. Robertson, "Capacitively-tuned split microstrip resonators for RFID barcodes," Proc. European. Microwave Conference, vol. 2, Italy, Oct. 2005.
[9] J. McVay, A. Hoorfar, and N. Engheta, "Space-filling curve RFID tags," Proc. IEEE Radio Wireless Symp., pp.199–202, Jan. 17–19, USA, 2006.
[10] L. Yang, R. Zhang, D. Staiculescu, C. P. Wong and M. M. Tentzeris, "A novel conformal RFID-enabled module utilizing inkjet-printed antennas and carbon nanotubes for gas-detection applications," IEEE Antennas and Wireless Propagation Letters, vol. 8, pp. 653-656, 2009.
[11] S., Shrestha, M. Balachandran, M. Agarwal, V.V., Phoha, K., Varahramyan, "A chipless RFID sensor system for cyber centric monitoring applications," IEEE Trans. Microwave Theory and Techniques, pp 1303-1309, vol. 57, no. 5, May 2009.
[12] A. C. Polycarpou, Introduction to the Finite Element Method in Electromagnetics, Morgan & Claypool, USA, 2006.
[13] S.J. Cooke, R. Shtokhamer, A.A. Mondelli, and B. Levush, "A finite integration method for conformal, structure-grid, electromagnetic simulation," Journal of computational physics, vol.215, pp. 321-347, 2006.
[14] T. Dissanayake and K. P. Esselle, "Prediction of the notch frequency of slot loaded printed UWB antennas," IEEE Trans. Antennas Propag., vol. 55, no. 12, pp. 3320–3325, Dec. 2007.
[15] E. Amin and N. Karmakar, "Development of a chipless RFID temperature sensor using cascaded spiral resonators," IEEE Sensors 2011 Conference, pp. 554 – 557, Ireland, Oct. 2011.

[16] http://cgtec.eu/wp-content/uploads/Stanyl_brochure_02.pdf.
[17] http://www.abgrp.co.uk/downloads/abg-datasheets/Nylon_4.6-Stanyl-.pdf.
[18] http://www1.isti.cnr.it/~salerno/Microonde/Taconic-laminate_material.pdf.
[19] G. T. Pawlikowski, "Effects of Polymer Material Variations on High Frequency Dielectric Properties," MRS 2009 Spring Meeting, vol. 1156, England, 2009.